

DiEC: Diffusion Embedded Clustering

Haidong Hu², Xiaoyu Zheng², Jin Zhou^{1,2,*}, Yingxu Wang², Rui Wang¹, Pei Dong²,
Shiyuan Han¹, Lin Wang², C. L. Philip Chen³, Tong Zhang³ and Yuehui Chen²

¹School of Artificial Intelligence, Shandong Women’s University, China

²Shandong Key Laboratory of Ubiquitous Intelligent Computing, University of Jinan, China

³School of Computer Science and Engineering, South China University of Technology, China
haidonghu.ml@gmail.com, zhoujin@sdwu.edu.cn

Abstract

Deep clustering methods typically rely on a single, well-defined representation for clustering. In contrast, pretrained diffusion models provide abundant and diverse multi-scale representations across network layers and noise timesteps. However, a key challenge is how to efficiently identify the most clustering-friendly representation in the layer×timestep space. To address this issue, we propose Diffusion Embedded Clustering (DiEC), an unsupervised framework that performs clustering by leveraging optimal intermediate representations from pretrained diffusion models. DiEC systematically evaluates the clusterability of representations along the trajectory of network depth and noise timesteps. Meanwhile, an unsupervised search strategy is designed for recognizing the Clustering-optimal Layer (COL) and Clustering-optimal Timestep (COT) in the layer×timestep space of pretrained diffusion models, aiming to promote clustering performance and reduce computational overhead. DiEC is fine-tuned primarily with a structure-preserving DEC-style KL-divergence objective at the fixed COL + COT, together with a random-timestep diffusion denoising objective to maintain the generative capability of the pretrained model. Without relying on augmentation-based consistency constraints or contrastive learning, DiEC achieves excellent clustering performance across multiple benchmark datasets.

1 Introduction

Clustering aims to uncover the intrinsic structure of unlabeled data. However, modern datasets are often high-dimensional, strongly nonlinear, and heavily contaminated by noise, making classical clustering methods that rely on shallow features and fixed distance metrics unreliable in practice [Liu *et al.*, 2016; Liu *et al.*, 2017]. By coupling neural representation learning with clustering objectives, deep clustering learns more semantic and noise-robust embeddings, demonstrating

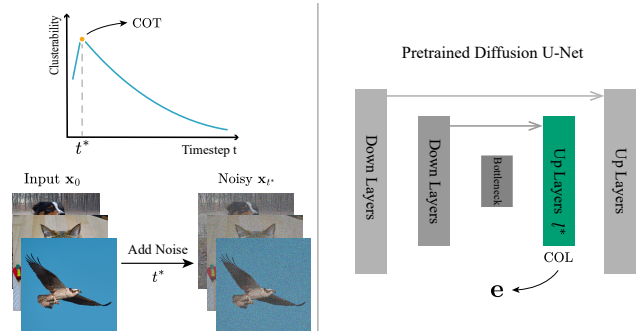


Figure 1: **Schematic of the feature extraction process in DiEC.** A clean image x_0 is perturbed with noise at the selected Clustering-Optimal Timestep (COT, t^*) to produce a noisy input x_{t^*} . This input, conditioned on the timestep embedding, is fed into the pretrained diffusion U-Net. The activation from the dynamically selected Clustering-Optimal Layer (COL, l^*) is subsequently extracted as the embedding representation e for downstream clustering.

good performance in applications such as image understanding, anomaly detection, and large-scale retrieval [Ren *et al.*, 2024].

Based on diverse network architectures, such as autoencoders (AE) [Xie *et al.*, 2016; Guo *et al.*, 2017a], variational autoencoders (VAE) [Jiang *et al.*, 2016; Yang *et al.*, 2019b], and generative adversarial networks (GAN) [Mukherjee *et al.*, 2019], embedding-based deep clustering methods typically learn representations by jointly optimizing reconstruction and clustering objectives. Nevertheless, these methods ultimately rely on a single, fixed latent representation for clustering, which lacks the dynamic adaptability and struggles to align with structural variations of data across different semantic scales.

Diffusion models, a significant breakthrough in generative artificial intelligence, excel at precisely modeling complex data distributions and capturing multi-scale semantic representations. Through forward noising and reverse denoising, they construct hierarchical features across different timesteps. A recent study [Wang *et al.*, 2024] further suggests that denoising representations can be spontaneously organized into multiple low-dimensional subspaces, naturally aligning with the needs of clustering. Yet, existing diffusion-based clustering research [Yan *et al.*, 2025; Uziel *et al.*, 2025; Yang *et al.*, 2024] has yet to fully exploit this potential, and in

*Corresponding author: Jin Zhou

particular lack systematic evaluation and effective selection of clustering-friendly representations across network layers and timesteps. Moreover, the high computational and time cost of diffusion inference remains a critical practical constraint.

Motivated by these insights, we propose **Diffusion Embedded Clustering (DiEC)**, an unsupervised framework that leverages internal representations of a pretrained diffusion U-Net for clustering. DiEC views the $\text{layer} \times \text{timestep}$ space as a representation trajectory and performs unsupervised evaluation to identify clustering-optimal readouts, namely the **Clustering-Optimal Layer (COL)** and the **Clustering-Optimal Timestep (COT)**. To alleviate interference between denoising and clustering objectives, DiEC introduces **residual feature decoupling** for effective task adaptation. For optimization, DiEC couples a DEC-style KL self-training objective with graph regularization to strengthen structural consistency, while retaining a random-timestep denoising reconstruction objective to preserve generative capability. Extensive experiments and ablations studies demonstrate that DiEC achieves excellent clustering performance on multiple benchmarks without relying on augmentation-based consistency constraints or contrastive learning. Our contributions are:

- DiEC provides a novel insight into diffusion-based clustering, revealing that effective feature selection within the multi-scale semantic representations of diffusion models is crucial for improving clustering performance.
- DiEC further develops an efficient, cost-aware, and label-free search strategy for recognizing clustering-friendly COL + COT in the $\text{layer} \times \text{timestep}$ space of pretrained diffusion models, aiming to promote clustering performance and reduce computational overhead.
- DiEC is fine-tuned primarily with a structure-preserving DEC-style KL-divergence clustering objective at the fixed COL + COT, together with a random-timestep diffusion denoising objective to maintain the generative capability of pretrained diffusion models.

2 Related Work

Embedding-based Deep Clustering. Embedding-based deep clustering methods aim to uncover latent cluster structure by learning a low-dimensional representation jointly with clustering objectives, enabling end-to-end optimization. AE-based approaches, represented by DEC [Xie *et al.*, 2016] and its extensions [Guo *et al.*, 2017a; Yang *et al.*, 2019b; Cai *et al.*, 2022; Zhang *et al.*, 2024; Guo *et al.*, 2017b], follow the classic “encode–cluster–refine” paradigm, typically combining reconstruction with clustering losses to preserve data structure while improving separability. However, purely deterministic encoders may overlook data uncertainty, and naively coupling reconstruction and clustering objectives can lead to optimization conflicts. VAE-based methods, such as VaDE [Jiang *et al.*, 2016], cast clustering as latent-variable inference by modeling embeddings as distributions and introducing mixture-based priors (e.g., GMM) in the latent space [Yang *et al.*, 2019a]. Recent variants further extend this

line to more challenging settings, including incomplete multi-view clustering and multimodal generative clustering [Xu *et al.*, 2024; Palumbo *et al.*, 2024]. GAN-based approaches such as ClusterGAN [Mukherjee *et al.*, 2019] leverage adversarial training and hybrid discrete–continuous latents to learn discriminative representations for clustering, while also inheriting practical issues of GAN training instability and the lack of explicit probabilistic inference. Overall, many existing pipelines rely on a fixed, single-scale readout for clustering, which limits flexibility in capturing structural variations across semantic scales. In contrast, our approach leverages diffusion models to construct a richer multi-scale representation space across network layers and diffusion timesteps, enabling more effective selection of clustering-friendly readouts.

Diffusion-Based Deep Clustering. Recent work [Wang *et al.*, 2024] suggests that denoising representations in diffusion models can spontaneously organize data into multiple low-dimensional subspaces, indicating strong potential for clustering. Building on this insight, diffusion-based clustering studies have rapidly emerged, broadly falling into three directions. First, several methods inject clustering signals as conditional information into the diffusion generative process to promote class-consistent generation and more separable cluster structures [Yan *et al.*, 2025; Palumbo *et al.*, 2024; Yang *et al.*, 2024; Yang *et al.*, 2022]. Second, other approaches treat the diffusion process as a feature extractor or a data augmentation mechanism to enhance clustering performance [Uziel *et al.*, 2025; Qiu *et al.*, 2024; Zhu *et al.*, 2025]. Third, diffusion-driven clustering has also been explored in practical application scenarios, such as hyperspectral imaging and ultrasound enhancement [Chen *et al.*, 2023; Chen *et al.*, 2025]. In contrast to prior diffusion clustering methods, we focus on systematically identifying clustering-friendly readouts from the intrinsic multi-scale representations of pretrained diffusion models, aiming to improve clustering quality while reducing computational overhead.

3 Background

Diffusion models. The core idea of diffusion models is to formulate generation as iterative denoising: a forward process gradually corrupts data with Gaussian noise, and a learned reverse process progressively removes noise to generate samples from the data distribution.

In DDPM [Ho *et al.*, 2020], the forward noising process is defined as a Markov chain that gradually corrupts a data sample $x_0 \sim q_{\text{data}}(x)$:

$$q(x_t | x_{t-1}) = \mathcal{N}\left(x_t \mid \sqrt{1 - \beta_t} x_{t-1}, \beta_t \mathbf{I}\right), \quad (1)$$

where $\{\beta_t\}_{t=1}^T$ is a predefined noise schedule and $t \in \{1, \dots, T\}$ denotes the diffusion timestep.

Let $\alpha_t = 1 - \beta_t$ and $\bar{\alpha}_t = \prod_{s=1}^t \alpha_s$. Then, the marginal distribution of x_t admits a closed-form expression

$$x_t = \sqrt{\bar{\alpha}_t} x_0 + \sqrt{1 - \bar{\alpha}_t} \epsilon, \quad \epsilon \sim \mathcal{N}(0, \mathbf{I}), \quad (2)$$

which shows that the noise level of x_t is fully governed by the timestep t .

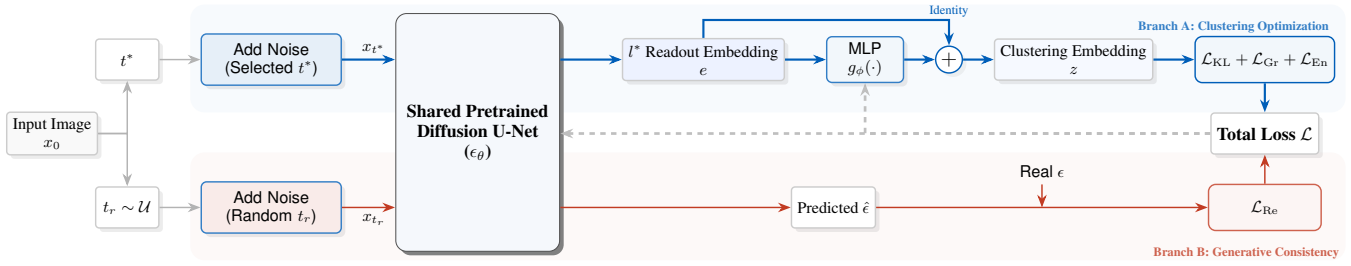


Figure 2: **Training framework of DiEC.** With $\text{COL}(l^*)$ and $\text{COT}(t^*)$ selected, Branch A optimizes clustering using $z = e + g_\phi(e)$ and $\mathcal{L}_{\text{KL}} + \mathcal{L}_{\text{Gr}} + \mathcal{L}_{\text{En}}$, while Branch B performs denoising at random t_r with \mathcal{L}_{Re} to preserve generative stability. Both form the total loss \mathcal{L} .

The reverse denoising process is parameterized as a Gaussian transition

$$p_\theta(x_{t-1} | x_t) = \mathcal{N}(x_{t-1} | \mu_\theta(x_t, t), \sigma_t^2 \mathbf{I}), \quad (3)$$

where the mean is expressed via a noise-prediction network ϵ_θ as

$$\mu_\theta(x_t, t) = \frac{1}{\sqrt{\alpha_t}} \left(x_t - \frac{\beta_t}{\sqrt{1 - \bar{\alpha}_t}} \epsilon_\theta(x_t, t) \right), \quad (4)$$

and the variance is fixed to the posterior value as

$$\sigma_t^2 = \tilde{\beta}_t = \frac{1 - \bar{\alpha}_{t-1}}{1 - \bar{\alpha}_t} \beta_t. \quad (5)$$

In practice, the noise prediction network $\epsilon_\theta(x_t, t)$ predicts the forward-process noise ϵ and is trained with a simple mean-squared error objective:

$$\mathcal{L}(\theta) = \mathbb{E}_{t, x_0, \epsilon} \left[\|\epsilon - \epsilon_\theta(x_t, t)\|_2^2 \right]. \quad (6)$$

The above MSE objective can be interpreted as a simplified variational bound on the data likelihood. At the sampling stage, starting from $x_T \sim \mathcal{N}(0, \mathbf{I})$, the reverse transition $p_\theta(x_{t-1} | x_t)$ is applied to progressively denoise samples and generate data.

DDPMs use discrete timesteps, while later work introduced continuous-time variants and an SDE-based view [Song *et al.*, 2020]. Recent studies have also explored Vision Transformers (ViTs) as diffusion backbones [Dosovitskiy, 2020; Peebles and Xie, 2023]. In this paper, we follow the discrete-time DDPM formulation with a U-Net denoiser to match our timestep-selection analysis.

Deep Embedded Clustering. Deep Embedded Clustering (DEC) is a method that simultaneously learns feature representations and cluster assignments [Xie *et al.*, 2016]. Given a set of embeddings $\{z_i\}_{i=1}^N$ and cluster centroids $\{\mu_k\}_{k=1}^K$, DEC defines the soft assignment via a Student’s t -distribution kernel as

$$q_{ik} = \frac{(1 + \|z_i - \mu_k\|^2 / \alpha)^{-\frac{\alpha+1}{2}}}{\sum_{k'=1}^K (1 + \|z_i - \mu_{k'}\|^2 / \alpha)^{-\frac{\alpha+1}{2}}}. \quad (7)$$

To emphasize high-confidence assignments and mitigate cluster-size imbalance, DEC constructs a target distribution $P = [p_{ik}]$ from $Q = [q_{ik}]$ as

$$p_{ik} = \frac{q_{ik}^2 / \sum_i q_{ik}}{\sum_{k'=1}^K (q_{ik'}^2 / \sum_i q_{ik'})}. \quad (8)$$

DEC then minimizes the KL divergence

$$\text{KL}(P \| Q) = \sum_i \sum_k p_{ik} \log \frac{p_{ik}}{q_{ik}} \quad (9)$$

for self-training, progressively sharpening the soft assignments and improving clustering consistency.

4 Diffusion Embedded Clustering

To leverage the multi-scale representations of diffusion models for clustering, DiEC first identifies the COL + COT by searching the layer \times timestep space of pretrained diffusion models, which guide the extraction, as illustrated in Fig. 1. Then, following Fig. 2, DiEC learns the embedding representations at the selected COL + COT through a shared pretrained U-Net backbone, and decouples the clustering representations via a lightweight residual network. Finally, DiEC performs clustering based on a DEC-style KL-divergence objective, supplemented by a random-timestep diffusion denoising objective to maintain the generative capability of pretrained diffusion models.

4.1 Locating Clustering-Friendly Diffusion Representations

Unsupervised Clusterability Metric. In the U-Net-based diffusion models, multi-scale semantic representations are indexed by both the network layer l and the noise timestep t . Given an unlabeled dataset $\mathcal{D} = \{x_{0,i}\}_{i=1}^N$ and the number of clusters K , $x_{t,i}$ denotes the noisy observation of the clean sample $x_{0,i}$ at diffusion timestep t . Then, we can obtain the embedding representations $\mathbf{E}_{l,t} = \{e_i^l(t)\}_{i=1}^N$ on U-Net layer l at timestep t as

$$e_i^l(t) = h_\theta^l(x_{t,i}, t). \quad (10)$$

The clusterability of these representations can be evaluated using the Scott Score, denoted as $\text{SS}(l, t)$, an unsupervised metric applied to assess clustering performance on data without ground-truth labels.

We run k -means on $\mathbf{E}_{l,t} = \{e_i^l(t)\}_{i=1}^N$ to yield cluster assignments $C_k^l(t)$ and centroids $\mu_k^l(t)$, and define the within-cluster scatter and the between-cluster scatter as

$$\mathbf{W}^l(t) = \sum_{k=1}^K \sum_{i \in C_k^l(t)} (e_i^l(t) - \mu_k^l(t)) (e_i^l(t) - \mu_k^l(t))^\top, \quad (11)$$

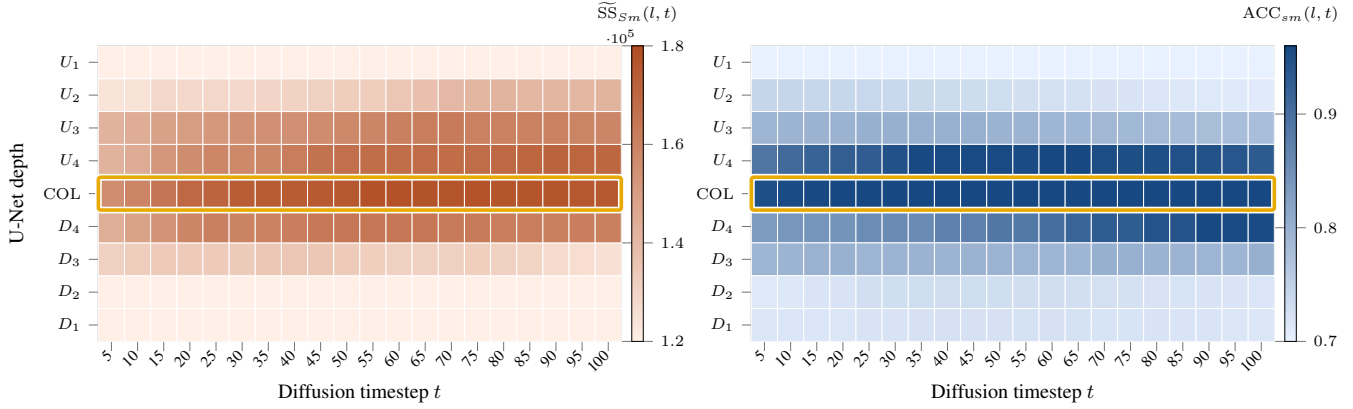


Figure 3: **Selection of COL on USPS.** The heatmaps display metrics across layers and timesteps. Left: Smoothed Scott Score (\widetilde{SS}_{Sm}). Right: ground-truth Smoothed Accuracy Score (ACC_{Sm}). The consistent alignment between the two metrics validates the COL selected by \widetilde{SS}_{Sm} . On this dataset, it is located at the bottleneck layer.

$$\mathbf{B}^l(t) = \sum_{k=1}^K |C_k^l(t)| (\mu_k^l(t) - \bar{e}^l(t)) (\mu_k^l(t) - \bar{e}^l(t))^\top, \quad (12)$$

where $\bar{e}^l(t) = \frac{1}{N} \sum_{i=1}^N e_i^l(t)$ denotes the global mean embedding across all samples.

Then, the Scott Score is defined as

$$SS(l, t) = N \left(\log \det \mathbf{T}^l(t) - \log \det \mathbf{W}^l(t) \right), \quad (13)$$

where $\mathbf{T}^l(t) = \mathbf{W}^l(t) + \mathbf{B}^l(t)$.

To reduce noise, we smooth the Scott Score along timesteps by a centered moving average as

$$SS_{Sm}(l, t) = \frac{1}{|\mathcal{N}(t)|} \sum_{\tau \in \mathcal{N}(t)} SS(l, \tau), \quad (14)$$

where $\mathcal{N}(t) = \{ \tau \in \mathcal{T} \mid |\tau - t| \leq \lfloor w/2 \rfloor \}$, \mathcal{T} is the set of evaluated timesteps and w is the window size.

In DiEC, this smoothed Scott Score $SS_{Sm}(l, t)$ serves as the unsupervised internal criterion for searching clustering-friendly representations.

Optimal Search for COL and COT. Based on the smoothed Scott Score, we design an Optimal Search strategy for identifying the COL and COT, denoted as l^* and t^* respectively. This strategy consists of two sequential stages: layer selection, followed by timestep selection.

In layer selection, considering the dimensional differences between representations across layers in the U-Net, we apply a PCA-based layer-wise alignment map $\mathcal{A}_l(\cdot)$ to obtain aligned embeddings $\widetilde{\mathbf{E}}_{l,t} = \{\tilde{e}_i^l(t)\}_{i=1}^N$, where $\tilde{e}_i^l(t) = \mathcal{A}_l(e_i^l(t))$, and evaluate its smoothed Scott Score as $\widetilde{SS}_{Sm}(l, t)$.

To obtain the robust evaluation for each layer, the timesteps ranked in the top- ρ percent (e.g. $\rho=20$) are utilized to identify the COL as

$$l^* = \arg \max_l \frac{1}{|\mathcal{T}_l^\rho|} \sum_{t \in \mathcal{T}_l^\rho} \widetilde{SS}_{Sm}(l, t), \quad (15)$$

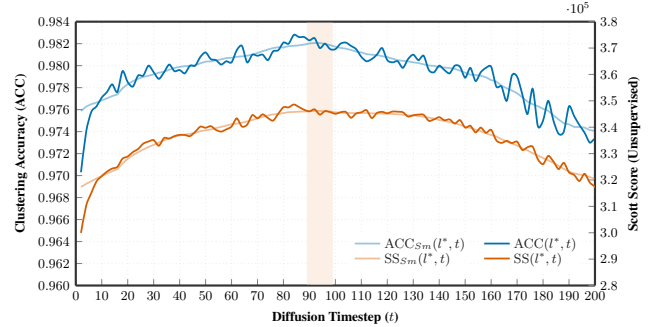


Figure 4: **Selection of COT on MNIST.** The evolution of the unsupervised Scott Score (SS and SS_{Sm} , orange) is closely aligned with the ground-truth clustering accuracy (ACC and ACC_{Sm} , blue) across diffusion timesteps on a fixed COL. Both metrics exhibit a distinct unimodal trend, with their smoothed peaks aligning in the same interval ($t \in [89, 99]$).

where $\mathcal{T}_l^\rho = \{ t \in \mathcal{T} \mid \text{rank}_t(\widetilde{SS}_{Sm}(l, t)) \leq \lceil \rho |\mathcal{T}| \rceil \}$.

From Fig. 3, we can see that the COL is located at the bottleneck layer on the USPS dataset (left panel). At the COL, the unsupervised Scott Score (SS) computed from the PCA-aligned inputs and the ground-truth clustering accuracy (ACC) exhibit similar trends. This observation confirms the effectiveness of the smoothed Scott Score as a reliable metric for identifying the COL.

In timestep selection, with l^* fixed, we evaluate clusterability directly on the native representations to remain consistent with training. The COT is then identified by

$$t^* = \arg \max_t \widetilde{SS}_{Sm}(l^*, t). \quad (16)$$

Fig. 4 shows the trajectory alignment between the unsupervised Scott Score (SS) and ground-truth clustering accuracy (ACC) across diffusion timesteps on the MNIST dataset. We also plot their smoothed values using the centered moving average mentioned above. It can be clearly seen that SS exhibits the same trend as ACC. In particular, by removing the effect of noise, their smoothed values are perfectly matched,

Algorithm 1 DiEC Joint Training Procedure

Input: Unlabeled dataset \mathcal{D} , Pretrained U-Net ϵ_θ with COL l^* , COT t^* , Residual MLP g_ϕ , Cluster number K , MaxEpochs E_{\max} , Update interval I_{target} .

- 1: **// Phase 1: Robust Initialization**
 - 2: Extract averaged embeddings $\{\bar{z}_i\}$ for all $x_i \in \mathcal{D}$ at selected (l^*, t^*) using M noise trials.
 - 3: Initialize centroids $\{\mu_k\}_{k=1}^K$ via k -means on $\{\bar{z}_i\}$.
 - 4: Construct graph affinity matrix \mathbf{S} (Eq. 20)
 - 5: **// Phase 2: Joint Optimization**
 - 6: **for** epoch = 1 to E_{\max} **do**
 - 7: **if** epoch % $I_{\text{target}} = 0$ **then**
 - 8: Update target distribution P (Eq. 8).
 - 9: **end if**
 - 10: **for** each sampled from \mathcal{D} **do**
 - 11: **// Branch A: Clustering-Aware Optimization**
 - 12: Sample noise $\epsilon \sim \mathcal{N}(0, \mathbf{I})$ and generate $x_{t^*, i}$.
 - 13: Extract features $e_i = h_\theta^{l^*}(x_{t^*, i}, t^*)$.
 - 14: Compute residual embedding (Eq. 18).
 - 15: Compute soft assignments Q (Eq. 7) and clustering loss \mathcal{L}_{KL} (Eq. 9).
 - 16: Compute graph constraint loss \mathcal{L}_{Gr} , \mathcal{L}_{En} (Eq. 21, 22).
 - 17: **// Branch B: Diffusion Consistency**
 - 18: Sample random timesteps $t_r \sim \mathcal{U}(\{1, \dots, T\})$.
 - 19: Generate noisy inputs $x_{t_r, i}$.
 - 20: Compute denoising loss \mathcal{L}_{Re} (Eq. 23).
 - 21: **// Joint Update**
 - 22: Update \mathbf{S} via Lagrange multipliers.
 - 23: $\mathcal{L}_{\text{total}} = \mathcal{L}_{\text{Re}} + \alpha\mathcal{L}_{\text{KL}} + \beta\mathcal{L}_{\text{Gr}} + \gamma\mathcal{L}_{\text{En}}$.
 - 24: Update $\theta, \phi, \{\mu_k\}$ via gradient descent: $\nabla \mathcal{L}_{\text{total}}$.
 - 25: **end for**
 - 26: **end for**
 - 27: **Output:** Cluster centroids $\{\mu_k\}$, assignments Q .
-

all reaching the maximum at the same timestep. This demonstrates that the smoothed Scott Score is a suitable evaluation metric for locating COT.

The complete procedure is detailed in Section A of the Appendix. Specifically, to mitigate diffusion stochasticity and reduce computational overhead, we estimate scores on a sample subset and average them over several independent noise realizations. This strategy substantially accelerates inference while maintaining high clustering accuracy.

4.2 Clustering-Aware Optimization

Given the features $e_i^{l^*}(t^*)$ extracted at (l^*, t^*) , we obtain clustering representations z_i through a lightweight residual mapping, and optimize a DEC-style KL self-training objective with graph regularization to strengthen cluster structure. Meanwhile, we add a standard denoising loss at a random timestep t_r , which helps maintain diffusion consistency and stabilize the representations.

Residual-decoupled embedding. To simplify the notation, we refer to $e_i^{l^*}(t^*)$ as e_i , where

$$e_i = h_\theta^{l^*}(x_{t^*, i}, t^*). \quad (17)$$

To reduce potential interference between the denoising objective and the clustering objective, we adopt a lightweight residual mapping $g_\phi(\cdot)$ (a two-layer ReLU MLP with matched input–output dimensions) to decouple clustering adaptation from the pretrained representation. The final clustering embedding is defined as

$$z_i = e_i + g_\phi(e_i). \quad (18)$$

This residual branch partially decouples clustering from denoising and enhances the expressiveness of the clustering loss.

Clustering objective. Given the clustering embeddings $\{z_i\}_{i=1}^N$, we adopt a DEC-style KL-divergence self-training objective. Since diffusion noising introduces stochasticity that can affect centroid initialization, we compute the mean embedding by averaging over M independent noise realizations at the selected layer l^* and timestep t^* as

$$\bar{z}_i = \frac{1}{M} \sum_{m=1}^M z_i^{(m)}. \quad (19)$$

Then, k -means is applied to $\{\bar{z}_i\}_{i=1}^N$ to initialize the centroids $\{\mu_k\}_{k=1}^K$. Based on $\{z_i\}_{i=1}^N$ and $\{\mu_k\}_{k=1}^K$, we compute the soft assignments Q via Eq. (7) and the target distribution P via Eq. (8). The clustering objective is then defined as their KL divergence in Eq. (9).

Adaptive graph regularization. To preserve local consistency in the embedding space, we introduce an adaptive graph regularization term. Specifically, we construct a row-normalized affinity matrix $\mathbf{S} = [s_{ij}]$ based on the k -NN neighborhood NB_i of each sample, with

$$s_{ij} = \begin{cases} \exp\left(-\frac{\|x_i - x_j\|_2^2}{\sigma}\right), & \text{if } x_j \in \text{NB}_i \\ 0, & \text{if } x_j \notin \text{NB}_i \end{cases}. \quad (20)$$

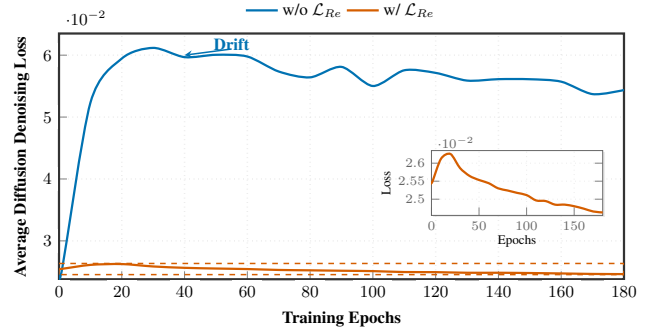


Figure 5: **Denoising stability analysis on USPS.** Without \mathcal{L}_{Re} (blue), the average diffusion denoising loss drifts, which impairs the generative capability of diffusion models. With \mathcal{L}_{Re} (red), the model maintains a low average denoising loss.

Table 2: **Quantitative comparison with state-of-the-art methods.** We primarily benchmark against **embedding-based** approaches for comparison, while also including **augmentation-consistency** methods to demonstrate the excellent clustering performance of our model. We report **ACC**, **NMI**, and **ARI** (%).

Method	MNIST			USPS			F-MNIST			CIFAR-10		
	ACC	NMI	ARI									
<i>Embedding-based Deep Clustering</i>												
DEC	84.7	79.1	74.9	73.3	70.6	63.7	53.6	59.1	42.0	25.1	13.6	7.8
IDEC	88.1	86.7	85.0	76.2	75.6	67.9	55.2	60.4	44.2	25.3	13.8	8.1
DCEC	88.5	87.6	84.3	78.0	81.8	73.6	62.7	65.9	54.0	28.7	26.5	16.9
VaDE	94.3	86.6	85.1	83.3	83.3	77.7	62.9	61.1	53.3	22.8	10.9	6.5
ClusterGAN	95.0	89.0	89.0	80.2	75.6	72.0	63.0	64.0	50.0	26.2	23.3	16.8
ClusterDDPM	97.7	94.0	93.2	81.3	83.8	76.1	70.5	66.1	56.9	30.5	17.3	15.7
<i>Reference: Augmentation Consistency Methods</i>												
IIC	99.2	97.9	97.8	81.8	85.9	81.1	65.7	63.4	52.4	61.7	51.3	41.1
DCCM	98.2	95.1	95.1	86.9	88.6	83.4	75.3	68.4	60.2	62.3	49.6	40.8
CC	96.6	93.2	93.1	91.5	90.0	83.2	70.8	67.5	56.5	79.0	70.5	63.7
DiEC (Ours)	99.5	98.5	98.0	98.5	97.0	95.7	79.7	75.5	66.5	71.4	61.5	56.1

We impose a graph constraint on the soft assignments Q to strengthen the cluster structure as

$$\begin{aligned} \mathcal{L}_{\text{Gr}} &= \sum_{i=1}^N \sum_{j \in \text{NB}_i} \sum_{k=1}^K s_{ij} (q_{ik} - q_{jk})^2, \\ \text{s.t.} \quad &\sum_{j \in \text{NB}_i} s_{ij} = 1, \quad s_{ij} \in [0, 1]. \end{aligned} \quad (21)$$

In addition, we introduce an entropy regularizer to prevent trivial solutions, formulated as

$$\mathcal{L}_{\text{En}} = \sum_{i=1}^N \sum_{j \in \text{NB}_i} s_{ij} \log s_{ij}. \quad (22)$$

Joint training with diffusion denoising. The update of the shared U-Net network only at timestep t^* may weaken its denoising performance at other timesteps, thereby impairing the overall stability of diffusion representations. Thus we introduce an additional noise-reconstruction branch at random timesteps t_r to maintain generative capability. Specifically, we sample $t_r \sim \mathcal{U}(\{1, \dots, T\})$ in each iteration and apply the standard forward noising to obtain $x_{t_r, i}$, and the noise-prediction MSE objective is then utilized to preserve the model’s generative capability, as defined by

$$\mathcal{L}_{\text{Re}} = \mathbb{E}_{t_r, \epsilon} \left[\frac{1}{N} \sum_{i=1}^N \|\epsilon - \epsilon_\theta(x_{t_r, i}, t_r)\|_2^2 \right]. \quad (23)$$

As shown in Fig. 5, \mathcal{L}_{Re} prevents drift during optimization and helps preserve generative capability across timesteps. Furthermore, Appendix Section B provides qualitative results that confirm the maintained generative quality.

4.3 Loss Function

We optimize the diffusion U-Net and the residual MLP module end-to-end with a weighted combination of objectives. The overall training objective is

$$\mathcal{L} = \mathcal{L}_{\text{Re}} + \alpha \mathcal{L}_{\text{KL}} + \beta \mathcal{L}_{\text{Gr}} + \gamma \mathcal{L}_{\text{En}}, \quad (24)$$

where \mathcal{L}_{Re} is the diffusion-consistency denoising reconstruction loss at random timesteps, \mathcal{L}_{KL} is the DEC-style clustering loss, \mathcal{L}_{Gr} and \mathcal{L}_{En} are the adaptive regularization terms. α , β , and γ are weighting hyperparameters that balance the relative contributions of the loss terms. The complete training procedure is provided in Algorithm 1.

5 Experiments

Datasets. We evaluate DiEC on four widely used benchmarks: MNIST, USPS, Fashion-MNIST, and CIFAR-10. MNIST and Fashion-MNIST each comprise 70,000 grayscale images at 28×28 resolution. USPS contains 9,298 grayscale images at 16×16 resolution, and CIFAR-10 consists of 60,000 color images at 32×32 resolution. The dataset statistics are summarized in Table 1.

Evaluation metrics. We evaluate clustering performance using clustering accuracy (ACC), normalized mutual information (NMI), and adjusted Rand index (ARI). Higher values indicate better clustering quality.

Table 1: Summary of datasets used in our experiments.

Dataset	Samples	Resolution	Classes
MNIST	70,000	28×28	10
USPS	9,298	16×16	10
Fashion-MNIST	70,000	28×28	10
CIFAR-10	60,000	32×32	10

Experimental Setup. We use a pretrained DDPM U-Net as the backbone. Table 2 compares DiEC with embedding-based baselines, including DEC, IDEC, DCEC, VaDE, ClusterGAN, and ClusterDDPM. To demonstrate the competitive advantages of our approach, we also compare with augmentation-consistency methods such as IIC [Ji *et al.*, 2019], DCCM [Wu *et al.*, 2019], and CC [Li *et al.*, 2021]. DiEC optimizes $\mathcal{L}_{\text{KL}} + \mathcal{L}_{\text{Gr}} + \mathcal{L}_{\text{En}}$ with the selected COL

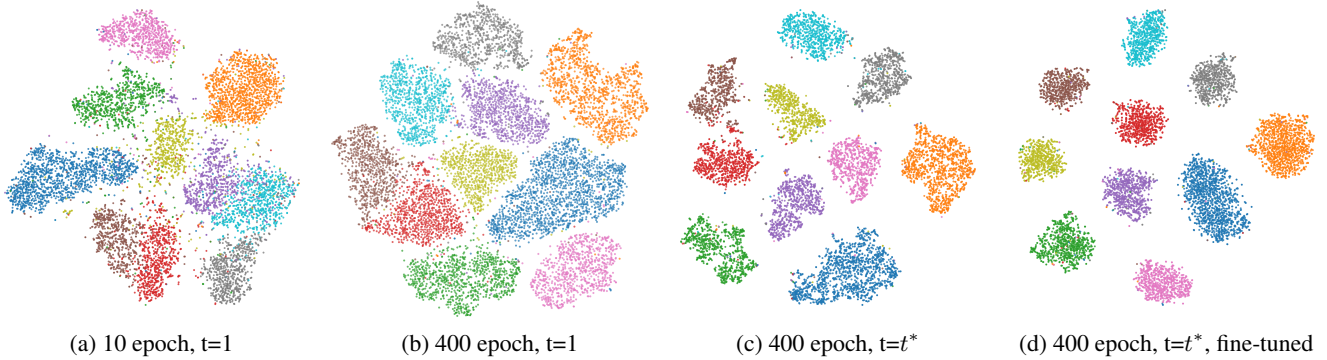


Figure 6: **Evolution of diffusion features for clustering on USPS.** t-SNE of COL embeddings across different pretraining stages and timesteps. We observe that clusters become more separable as diffusion pretraining progresses. Furthermore, switching from $t=1$ to the optimal timestep t^* reveals significantly clearer structures, which are finally sharpened by DiEC optimization.

+ COT, and the standard denoising loss \mathcal{L}_{Re} at random timesteps. Ground-truth labels are reserved solely for evaluation, and the number of clusters K is predefined. Images are normalized for diffusion input.

Main Results. Table 2 shows that DiEC achieves excellent clustering performance, outperforming embedding-based baselines, including DEC, IDEC, DCEC, VaDE, and ClusterGAN, as well as the diffusion-based ClusterDDPM. Moreover, DiEC outperforms augmentation-consistency methods, including IIC, DCCM, and CC, especially on grayscale benchmarks such as MNIST, USPS, and Fashion-MNIST.

Ablation Study. Table 3 reports the contribution of each component on the USPS dataset. First, compared with randomly selection of a layer and timestep (ID 1), the identified COL (ID 2) provides a 4.6% improvement in ACC. Next, by fixing the timestep to COT, ID 3 brings a large improvement in clustering performance, resulting in an ACC of 96.83%. This confirms the importance of layer and timestep selection, and the effectiveness of the smoothed Scott Score serving as a reliable evaluation metric for locating COL and COT. Then, the subsequent integration of KL self-training, residual decoupling, and adaptive graph regularization (ID 4-6) further refines the feature space, thereby enhancing the clustering performance. Finally, the employment of random-timestep diffusion consistency (ID 7) further refines the representation, culminating in the performance of 98.49% in ACC, 96.95% in NMI, and 95.65% in ARI.

Table 3: **Ablation analysis on USPS.** Starting from a random baseline averaged over 50 runs (random layer and timestep), we incrementally add COL/COT selection and the DiEC objectives. The COL variant is also averaged over 50 runs by fixing the layer to COL while randomly sampling timesteps. Here, **Res.** denotes Residual Decoupling. The full model (ID 7) achieves superior performance.

ID	Methods	ACC(%)		NMI(%)		ARI(%)	
		Val.	Δ	Val.	Δ	Val.	Δ
1	Baseline: Random t and l	40.64	–	25.67	–	29.60	–
2	+ Selected l^* (COL)	45.21	$\uparrow 4.57$	28.04	$\uparrow 2.37$	30.39	$\uparrow 0.79$
3	+ Selected t^* (COT)	96.83	$\uparrow 51.62$	93.82	$\uparrow 65.78$	92.21	$\uparrow 61.82$
4	+ Direct Fine-tuning (\mathcal{L}_{KL})	97.11	$\uparrow 0.28$	94.31	$\uparrow 0.49$	92.66	$\uparrow 0.45$
5	+ Residual Decoupling (Res.)	97.21	$\uparrow 0.10$	94.46	$\uparrow 0.15$	92.83	$\uparrow 0.17$
6	+ Graph Regularization ($\mathcal{L}_{Gr} + \mathcal{L}_{En}$)	98.37	$\uparrow 1.16$	96.76	$\uparrow 2.30$	95.45	$\uparrow 2.62$
7	+ Diffusion Consistency (\mathcal{L}_{Re})	98.49	$\uparrow 0.12$	96.95	$\uparrow 0.19$	95.65	$\uparrow 0.20$
Δ (Full – Baseline)		–	$\uparrow 57.85$	–	$\uparrow 71.28$	–	$\uparrow 66.05$

Qualitative Analysis. Fig. 6 visualizes the evolution of USPS embeddings via t-SNE, utilizing features extracted from the COL. Fig. 6 (a) and Fig. 6 (b) display the results at diffusion timestep $t=1$. Despite the convergence of pretraining after 400 epochs, the cluster boundaries remain relatively ambiguous. In contrast, switching to the identified COT leads to more dispersed class distributions Fig. 6 (c). Finally, the full DiEC fine-tuning at the COT further refines the structure, yielding highly separable clusters Fig. 6 (d).

6 Conclusion

In this paper, DiEC, a diffusion-based deep clustering framework, is proposed to directly leverage clustering-friendly embedding representations from pretrained diffusion models for unsupervised clustering. A complementary optimal search strategy is therefore designed to recognize COL and COT in the layer \times timestep space through an unsupervised Scott Score criterion. Then, DiEC performs clustering on extracted representations with DEC-style KL-divergence objective, supplemented by a random-timestep diffusion denoising objective to maintain the generative capability of pretrained diffusion models. Experiments and ablation studies on four benchmarks demonstrate the superiority of DiEC

over embedding-based and augmentation-consistency clustering methods, revealing that the effective feature selection based on identified COL + COT is crucial for improving clustering performance.

Acknowledgments

This work was supported in part by the National Natural Science Foundation of China under Grants No. 62273164 and No. 62373164, the Project of Central Government Guides Local Program under Grant YDZX2024075, the Taishan Scholars Program of Shandong Province under Grant tsqn202507271, and the Taishan Experts Program under Grant tscy20241154.

A Optimal Search algorithm

Optimal Search adopts a two-stage strategy. In both stages, we evaluate candidate representations on a sampled subset and reduce diffusion stochasticity by averaging over multiple noise trials, as shown in Algorithm A1.

In Stage 1, we sample a subset \mathcal{D}_s and evaluate each layer over a timestep set \mathcal{T} . We then smooth the scores across timesteps and compute a layer-level score by averaging the top- ρ fraction of each layer’s timestep-level scores, which is used to select the COL.

In Stage 2, we fix the selected COL and evaluate the same timestep set \mathcal{T} to identify the COT, again using smoothed scores for robust selection, and we stop early if the score does not improve for P consecutive timesteps.

Algorithm A1 Optimal Search for COL and COT

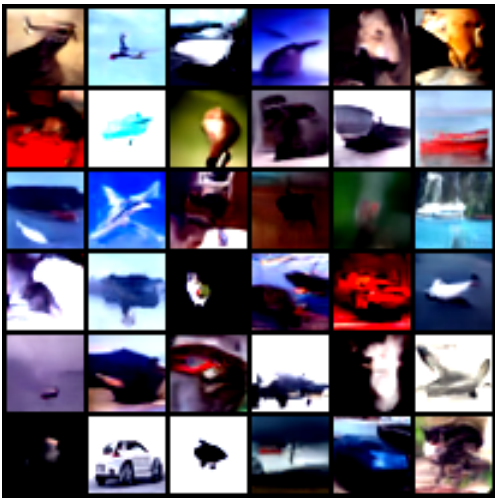
Input: Dataset \mathcal{D} ; pretrained feature extractor $\{h_\theta^l\}_{l \in \mathcal{L}}$; timestep range $[1, T_s]$; stride Δt ; subset size m ; noise trials R ; PCA dim d ; smoothing window w ; top fraction ρ ; patience P

Output: COL l^* , COT t^*

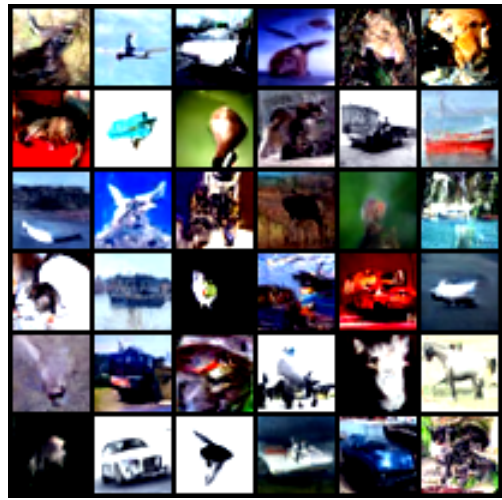
```

1: Sample subset  $\mathcal{D}_s \subset \mathcal{D}$  with  $|\mathcal{D}_s| = m$ 
2:  $\mathcal{T} \leftarrow \{1, 1 + \Delta t, 1 + 2\Delta t, \dots, T_s\}$ 
3: Stage 1: layer selection
4: for  $l \in \mathcal{L}$  do
5:   for  $t \in \mathcal{T}$  do
6:     for each  $x_{0,i} \in \mathcal{D}_s$  do
7:       Sample noises  $\{\epsilon^{(r)}\}_{r=1}^R$  and form  $\{x_{t,i}^{(r)}\}_{r=1}^R$ 
8:        $e_i^{l,(r)}(t) \leftarrow h_\theta^l(x_{t,i}^{(r)}, t)$ 
9:        $\bar{e}_i^l(t) \leftarrow \frac{1}{R} \sum_{r=1}^R e_i^{l,(r)}(t)$ 
10:    end for
11:     $\mathbf{E}_{l,t} \leftarrow \{\bar{e}_i^l(t)\}_{x_{0,i} \in \mathcal{D}_s}$ 
12:     $\tilde{\mathbf{E}}_{l,t} \leftarrow \ell_2\text{-Norm}(\text{PCA}_d(\mathbf{E}_{l,t}))$ 
13:     $\widetilde{\text{SS}}(l, t) \leftarrow \text{Scott}(\tilde{\mathbf{E}}_{l,t})$ 
14:    end for
15:     $\widetilde{\text{SS}}_{Sm}(l, t) \leftarrow \text{MovAvg}(\widetilde{\text{SS}}(l, t), w)$ 
16:     $\hat{S}_\rho(l) \leftarrow \text{MeanTop}_\rho(\widetilde{\text{SS}}_{Sm}(l, t))$ 
17:  end for
18:  $l^* \leftarrow \arg \max_{l \in \mathcal{L}} \hat{S}_\rho(l)$ 
19: Stage 2: timestep selection
20:  $S_{\max} \leftarrow -\infty$ ;  $t^* \leftarrow 0$ ;  $c \leftarrow 0$ 
21: for  $t \in \mathcal{T}$  do
22:   for each  $x_{0,i} \in \mathcal{D}_s$  do
23:     Sample noises  $\{\epsilon^{(r)}\}_{r=1}^R$  and form  $\{x_{t,i}^{(r)}\}_{r=1}^R$ 
24:      $e_i^{(r)}(t) \leftarrow h_\theta^{l^*}(x_{t,i}^{(r)}, t)$ 
25:      $\bar{e}_i(t) \leftarrow \frac{1}{R} \sum_{r=1}^R e_i^{(r)}(t)$ 
26:    end for
27:     $\mathbf{E}_{l^*,t} \leftarrow \{\bar{e}_i(t)\}_{x_{0,i} \in \mathcal{D}_s}$ 
28:     $SS(l^*, t) \leftarrow \text{Scott}(\mathbf{E}_{l^*,t})$ 
29:     $SS_{Sm}(l^*, t) \leftarrow \text{OnlineMovAvg}(SS(l^*, t), t, w)$ 
30:    if  $SS_{Sm}(l^*, t) > S_{\max}$  then
31:       $S_{\max} \leftarrow SS_{Sm}(l^*, t)$ ;  $t^* \leftarrow t$ 
32:    end if
33:    else
34:       $c \leftarrow c + 1$ 
35:    end if
36:    if  $c \geq P$  then
37:      break
38:    end if
39:  end for
40: return  $(l^*, t^*)$ 

```



(a) Pretrained diffusion model



(b) After DiEC fine-tuning

Figure A1: **Qualitative samples on CIFAR-10 (before vs. after DiEC).** The two grids are generated using the same sampling configuration, and the diffusion model’s generative capability is well preserved after fine-tuning, supporting the role of \mathcal{L}_{Re} in maintaining generative consistency.

B Qualitative Comparison of Generation

We evaluated the generative capability of the proposed DiEC on CIFAR-10. Fig. A1 presents images generated by the pre-trained and fine-tuned models from the same set of samples. Both models exhibit high image fidelity and diversity. Notably, the images generated by the fine-tuned DiEC contain more details, which validates the effectiveness of our reconstruction objective \mathcal{L}_{Re} in maintaining generative consistency.

References

- [Cai *et al.*, 2022] Jinyu Cai, Jicong Fan, Wenzhong Guo, Shiping Wang, Yunhe Zhang, and Zhao Zhang. Efficient deep embedded subspace clustering. In *Proceedings of the IEEE/CVF conference on computer vision and pattern recognition*, pages 1–10, 2022.
- [Chen *et al.*, 2023] Jiabin Chen, Shujun Liu, Zhongbiao Zhang, and Huajun Wang. Diffusion subspace clustering for hyperspectral images. *IEEE Journal of Selected Topics in Applied Earth Observations and Remote Sensing*, 16:6517–6530, 2023.
- [Chen *et al.*, 2025] Nuo Chen, Yongquan Zhang, Chenchen Fan, Wei Zhao, Changmiao Wang, and Hai Wang. DiffusionClusNet: Deep clustering-driven diffusion models for ultrasound image enhancement. *IEEE Transactions on Consumer Electronics*, 2025.
- [Dosovitskiy, 2020] Alexey Dosovitskiy. An image is worth 16x16 words: Transformers for image recognition at scale. *arXiv preprint arXiv:2010.11929*, 2020.
- [Guo *et al.*, 2017a] Xifeng Guo, Long Gao, Xinwang Liu, and Jianping Yin. Improved deep embedded clustering with local structure preservation. In *Ijcai*, volume 17, pages 1753–1759, 2017.
- [Guo *et al.*, 2017b] Xifeng Guo, Xinwang Liu, En Zhu, and Jianping Yin. Deep clustering with convolutional autoencoders. In *International conference on neural information processing*, pages 373–382. Springer, 2017.
- [Ho *et al.*, 2020] Jonathan Ho, Ajay Jain, and Pieter Abbeel. Denoising diffusion probabilistic models. *Advances in neural information processing systems*, 33:6840–6851, 2020.
- [Ji *et al.*, 2019] Xu Ji, Joao F Henriques, and Andrea Vedaldi. Invariant information clustering for unsupervised image classification and segmentation. In *Proceedings of the IEEE/CVF international conference on computer vision*, pages 9865–9874, 2019.
- [Jiang *et al.*, 2016] Zhuxi Jiang, Yin Zheng, Huachun Tan, Bangsheng Tang, and Hanning Zhou. Variational deep embedding: An unsupervised and generative approach to clustering. *arXiv preprint arXiv:1611.05148*, 2016.
- [Li *et al.*, 2021] Yunfan Li, Peng Hu, Zitao Liu, Dezhong Peng, Joey Tianyi Zhou, and Xi Peng. Contrastive clustering. In *Proceedings of the AAAI conference on artificial intelligence*, volume 35, pages 8547–8555, 2021.
- [Liu *et al.*, 2016] Xinwang Liu, Yong Dou, Jianping Yin, Lei Wang, and En Zhu. Multiple kernel k-means clustering with matrix-induced regularization. In *Proceedings of the AAAI conference on artificial intelligence*, volume 30, 2016.
- [Liu *et al.*, 2017] Weiwei Liu, Xiaobo Shen, and Ivor Tsang. Sparse embedded k -means clustering. *Advances in neural information processing systems*, 30, 2017.
- [Mukherjee *et al.*, 2019] Sudipto Mukherjee, Himanshu Asnani, Eugene Lin, and Sreeram Kannan. Clustergan: Latent space clustering in generative adversarial networks. In *Proceedings of the AAAI conference on artificial intelligence*, volume 33, pages 4610–4617, 2019.
- [Palumbo *et al.*, 2024] Emanuele Palumbo, Laura Manduchi, Sonia Laguna, Daphné Chopard, and Julia E Vogt. Deep generative clustering with multimodal diffusion variational autoencoders. In *The Twelfth International Conference on Learning Representations*, 2024.
- [Peebles and Xie, 2023] William Peebles and Saining Xie. Scalable diffusion models with transformers. In *Proceedings of the IEEE/CVF international conference on computer vision*, pages 4195–4205, 2023.
- [Qiu *et al.*, 2024] Liping Qiu, Qin Zhang, Xiaojun Chen, and Shaotian Cai. Multi-level cross-modal alignment for image clustering. In *Proceedings of the AAAI Conference on Artificial Intelligence*, volume 38, pages 14695–14703, 2024.
- [Ren *et al.*, 2024] Yazhou Ren, Jingyu Pu, Zhimeng Yang, Jie Xu, Guofeng Li, Xiaorong Pu, Philip S Yu, and Lifang He. Deep clustering: A comprehensive survey. *IEEE transactions on neural networks and learning systems*, 36(4):5858–5878, 2024.
- [Song *et al.*, 2020] Yang Song, Jascha Sohl-Dickstein, Diederik P Kingma, Abhishek Kumar, Stefano Ermon, and Ben Poole. Score-based generative modeling through stochastic differential equations. *arXiv preprint arXiv:2011.13456*, 2020.
- [Uziel *et al.*, 2025] Roy Uziel, Irit Chelly, Oren Freifeld, and Ari Pakman. Clustering via self-supervised diffusion. *arXiv preprint arXiv:2507.04283*, 2025.
- [Wang *et al.*, 2024] Peng Wang, Huijie Zhang, Zekai Zhang, Siyi Chen, Yi Ma, and Qing Qu. Diffusion models learn low-dimensional distributions via subspace clustering. *arXiv preprint arXiv:2409.02426*, 2024.
- [Wu *et al.*, 2019] Jianlong Wu, Keyu Long, Fei Wang, Chen Qian, Cheng Li, Zhouchen Lin, and Hongbin Zha. Deep comprehensive correlation mining for image clustering. In *Proceedings of the IEEE/CVF international conference on computer vision*, pages 8150–8159, 2019.
- [Xie *et al.*, 2016] Junyuan Xie, Ross Girshick, and Ali Farhadi. Unsupervised deep embedding for clustering analysis. In *International conference on machine learning*, pages 478–487. PMLR, 2016.
- [Xu *et al.*, 2024] Gehui Xu, Jie Wen, Chengliang Liu, Bing Hu, Yicheng Liu, Lunke Fei, and Wei Wang. Deep variational incomplete multi-view clustering: Exploring shared clustering structures. In *Proceedings of the AAAI conference on artificial intelligence*, volume 38, pages 16147–16155, 2024.
- [Yan *et al.*, 2025] Jie Yan, Jing Liu, and Zhong-yuan Zhang. ClusterDDPM: an EM clustering framework with denoising diffusion probabilistic models. *Information Sciences*, page 122518, 2025.
- [Yang *et al.*, 2019a] Linxiao Yang, Ngai-Man Cheung, Jiaying Li, and Jun Fang. Deep clustering by gaussian mixture variational autoencoders with graph embedding. In

Proceedings of the IEEE/CVF international conference on computer vision, pages 6440–6449, 2019.

- [Yang *et al.*, 2019b] Xu Yang, Cheng Deng, Feng Zheng, Junchi Yan, and Wei Liu. Deep spectral clustering using dual autoencoder network. In *Proceedings of the IEEE/CVF conference on computer vision and pattern recognition*, pages 4066–4075, 2019.
- [Yang *et al.*, 2022] Xiaojiang Yang, Junchi Yan, Yu Cheng, and Yizhe Zhang. Learning deep generative clustering via mutual information maximization. *IEEE Transactions on Neural Networks and Learning Systems*, 34(9):6263–6275, 2022.
- [Yang *et al.*, 2024] Ruohong Yang, Peng Hu, Xi Peng, Xiting Liu, and Yunfan Li. DiFiC: Your diffusion model holds the secret to fine-grained clustering. *arXiv preprint arXiv:2412.18838*, 2024.
- [Zhang *et al.*, 2024] Runxin Zhang, Yu Duan, Feiping Nie, Rong Wang, and Xuelong Li. Unsupervised deep embedding for fuzzy clustering. *IEEE Transactions on Fuzzy Systems*, 2024.
- [Zhu *et al.*, 2025] Yanjiao Zhu, Qilin Li, Wanquan Liu, and Chuancun Yin. Diffusion process with structural changes for subspace clustering. *Pattern Recognition*, 158:111066, 2025.